PROCEEDINGS, 43rd Workshop on Geothermal Reservoir Engineering
Stanford University, Stanford, California, February 12-14, 2018
SGP-TR-213

Estimation of Static Temperature Distribution by Means of Audio-Magnetotelluric Data

Maryadi Maryadi[1,2] and Hideki Mizunaga[1]

[1]Department of Earth Resources Engineering, Kyushu University, Fukuoka, Japan, 819-0395

[2]Program Studi Geofisika, Fakultas Matematika dan Ilmu Pengetahuan Alam, Universitas Indonesia, Depok, Indonesia, 16424

maryadi@mine.kyushu-u.ac.jp

Keywords: temperature estimation, resistivity, geothermometry, artificial neural network, audio-magnetotelluric

ABSTRACT

Knowledge about the temperature distribution within the geothermal system is considered significant in geothermal exploration. The study is mainly done by the costly well drilling, and/or a number of indirect geothermometers which only provide limited information. In this work, the static geothermal heat distribution was analyzed based on the proven relation between resistivity and temperature. The temperature was estimated after the application of indirect electromagnetic geothermometer which employs the calibrated artificial neural network. A validation test of this method was satisfying as the predicted temperature profiles were diverse to the measured ones with around 10% of relative error. Following the results, a full assessment of subsurface temperature was performed, approximated from a three-dimensional audio-magnetotelluric inversion result. The varying geothermal gradients within the area and the resistivity anomalies provide an idea about the existing geothermal structure and the fluid-heating system under the field examined in this study. As a conclusion, forecasting the temperature from the resistivity value can be considered as a quick and reliable method to massively explore the geothermal resource potential.

1. INTRODUCTION

Geothermometry has been an essential study in geothermal exploration which is purposing to get the subsurface temperature information rather than using the costly borehole logging. The study is based on the association between the rock-fluid conditions and the formation temperature. Indirect geothermometer is a significant part of the geochemical analysis. Geothermometer based on alteration mineral is one of the commonly used methods. Some other types make use of the gas and isotope content of the material. The temperature at the unreachable depths, usually the depth of reservoir zone, is mainly predicted by the presence of chemical elements in geothermal fluids or rock samples. The degree of heat is indirectly estimated from the established empirical formulas which also, to some extent, require lithological information.

Electromagnetic geothermometry is a recently designed approach to do such a task. This method does not need any sample *in situ*, nor prior lithological information. The estimation is based on electromagnetic data which has been calibrated through the application of artificial neural network in advance, as introduced by Spichak (2006). By using the electromagnetic-based geothermometer, the relation is learned through the artificial neural network (ANN) so that the network will be able to predict the temperature from the given resistivity value (Spichak et al., 2011). The reliability of this approach had been evaluated in several studies (e.g., Akpan et al., 2014; Spichak and Zakharova, 2009). A comprehensive discussion about this method is summarized in a book by Spichak and Zakharova (2015). However, the number of research proving the trustworthiness of this approach remains small.

In this study, this approximation was assessed and applied to give a principal idea about the subsurface temperature condition. Concerning the model resolution, audio-frequency magnetotelluric (AMT) method was used to enhance the data density. Following the result of the temperature estimation, joint interpretation of the resistivity and the static temperature anomaly was also carried out to delineate a proper model of the existing geothermal system. The content of this paper is adapted from the preliminary study in an extended abstract by Maryadi and Mizunaga (2017).

2. GEOTHERMAL FIELD DATA

The AMT and temperature data used in this work was acquired from the exploratory studies of an active geothermal field in Japan which has been producing electricity for more than 20 years. To analyze the possibility of the reservoir expansion, an AMT survey consists of more than 60 measurement sites was carried out. A number of wells were also drilled throughout the area to get a convincing knowledge related to the geological condition and heat propagation. The depth of penetration of the wells is around 1,500 m in average. The locations of the AMT stations and the borehole drilling sites are illustrated on the map in Figure 1. The map was rotated 25° NW so that the station location can be easily recognizable in the 3-D resistivity maps showed later in the last section.

Six available AMT-temperature datasets were used as the network learning basis (SK201-BT1, SK302-BT2, SK106-BT3, SK505-BT4, SK707-BT5 and SK509-BT9). The resistivity resulted from inversion process, and its spatial coordinates were tied with the temperature profile from the adjacent borehole thermogram as one dataset. This AMT-temperature dataset was then employed as input and output, respectively so that the network could learn the relationship behavior. Each of them carries essential information about the subsurface condition. Therefore, it is still necessary to analyze both data individually before using them for teaching the network as well as performing the prediction. The geological investigation had also been carried out. Some of the conclusions are explained beforehand so that the necessary information about the subsurface condition is understandable.

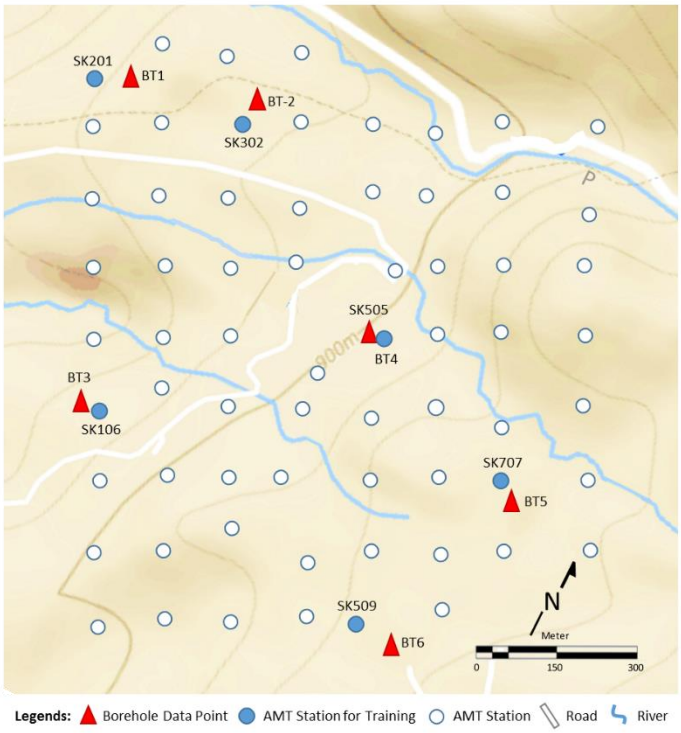

Figure 1: Location map of the study area (after Maryadi and Mizunaga, 2017).

2.1 Surface Geology and Well Log Data

The studied geothermal field is located at a highland, around 900 m above sea level. The area is covered by volcanic materials which came out from the mountain complex located approximately 5 km to the east since Pleistocene epoch. The deeper formation is mainly composed of sandstone and shale which is taking a role as the basement rock. It was presumed that the present geothermal activity is primarily due to the presence of the inactive volcanic body related to the nearby volcanic mountain. From the exploratory wells, the measured temperature below the area was estimated around 230 °C in average. The previous geological investigation suggested that the geothermal fluids are infiltrating downward through the existing fracture systems within the surrounding graben-like structure. The fluids penetrate to the porous volcanic body approximately around 1-2 km. They circulate and being heated by the heat source before going upward through the other fault structure.

The major faults in this geothermal area are mainly elongated from west-southwest to east-southeast. These structures have a strike of about 60° NE. One of them is located in the north-western vicinity with the steep dip angle of 70° facing the north. Another structure appears in the south-southwestern part outside the area and the fault plane dips 60° to the south. The strike and dip information were obtained from thermo-remnant magnetism analysis of the extracted cores. There are a number of fumarole discharges in this area. Those manifestations are aligned parallel with the principal angle of the fault structures which could be evidence that the faults are meaningful for the outflow movement and general circulation of the geothermal fluid.

2.2 AMT Data Processing

AMT method employs high-frequency range starts from 10^{-1} to 10^{4} Hz. This range enables the signal to propagate up to an approximated depth of 2,000 m. The data were undergoing the pre-inversion process such as coherence analysis, distortion removal, and static shift correction to minimalize the prediction inaccuracy due to the propagation of errors. This subsection is only focusing on the processing steps of the AMT training dataset mentioned before. The quality of the training data is vital as the neural network will count on them as the foundation for the prediction.

2.2.1 Dimensionality Analysis

Delineating the electrical resistivity model is highly depending on the distortion level in the data, or known as dimensionality. The measured MT or AMT data are commonly affected by distortions due to local inhomogeneity or induction by three-dimensional structures. Each dimensionality model has its own characteristic. Therefore, one should take this property into consideration in the subsurface resistivity modeling. The three-dimensional distortion level in the impedance tensor should be checked, as the ANN will learn about how the resistivity related with temperature based on its 1-D inversion result. The dimensionality analysis of the AMT stations inside the profile was evaluated by using the Swift's skew (κ) with the following formula

$$\kappa = \left| \frac{Z_{xx} + Z_{yy}}{Z_{xy} - Z_{yx}} \right| , \quad (1)$$

where Z_{xx}, Z_{yy}, Z_{xy}, and Z_{yx} are the elements of impedance tensor (Swift, 1967). The skew value of 1-D characterized subsurface should be zero and getting larger as the dimensionality is getting complex. A threshold value of 0.2 was chosen to compromise the occurrences of small distortion in the impedance tensor. However, the low κ skew value does not always indicate a free distortion structure. Therefore, another analysis to support the result of Swift's skew is necessary.

The ellipticity of the phase tensor was analyzed. The phase tensor of the magnetotelluric signal, introduced by Caldwell et al. (2004) is basically illustrated as an ellipse whose form is determined by its coordinate invariants: maximum phase (Φ_{max}), minimum phase (Φ_{min}), and the skew angle (β). The elongation of the ellipse could also indicate the primary geoelectrical structure. In the one-dimensional case, the maximum and minimum values in the phase tensor are expected to have no difference so that the ellipse will form like a circle with a skew angle of zero. A quantitative analysis of the ellipticity (E) is formulated by

$$E = \frac{\Phi_{max} - \Phi_{min}}{\Phi_{min} + \Phi_{min}} . \quad (2)$$

To be regarded as 1-D structure, the ellipticity measured in the location should be less than 0.1 (Bibby et al., 2005). The results of Swift's skew and ellipticity analysis are shown in Figure 2. Generally speaking, both skew values and ellipticity are considered small, while in some frequencies the values are quite high in the northern part and are relatively lower in the southern and eastern parts. Taking this result into account, the use of a 1-D resistivity model of the six AMT training data for estimating the temperature up to the desired depth is considered acceptable.

2.2.2 One-Dimensional AMT Inversion

Thermogram data was recorded for every 10 m interval downwards. To counterbalance the resolution of temperature data, the subsurface resistivity data should be modeled smoothly. In this work, Occam 1-D inversion algorithm was adopted (Constable, 1987). The inversion was carried out using the source code developed by Key (2009). The inversion was based on the determinant of the impedance tensor.

The initial model depth was 2 km occupied 30 layers which are elongated with depth starting from 10 m thickness at the surface layer. The inversion results of the AMT data used for training are shown in Figure 3. The RMS misfit is generally small, about 4% in average. From the 1-D inversion result, it could be inferred that for the shallow depth the resistivity is predominantly high in every station which is exceeding 100 Ωm. The thickness of this overlying resistive layer is, however, varying from one location to another. For the upper three inversion results in Figure 3, the maximum depth of this high resistivity deposit is, to some extent, shallower than the one recorded for the other three sites.

In the subsequent zone, all the resistivity inversion results indicate the appearance of the conductive layer. This is most probably the representation of the impermeable cap rock. Since each AMT station has a different thickness of the resistive top layer, this conductive impermeable layer was also encountered at the different depth. For the AMT station SK201, SK302, and SK106 the lowest resistivity value is recorded at 400 m depth. For the other three stations, this anomaly is found below that depth.

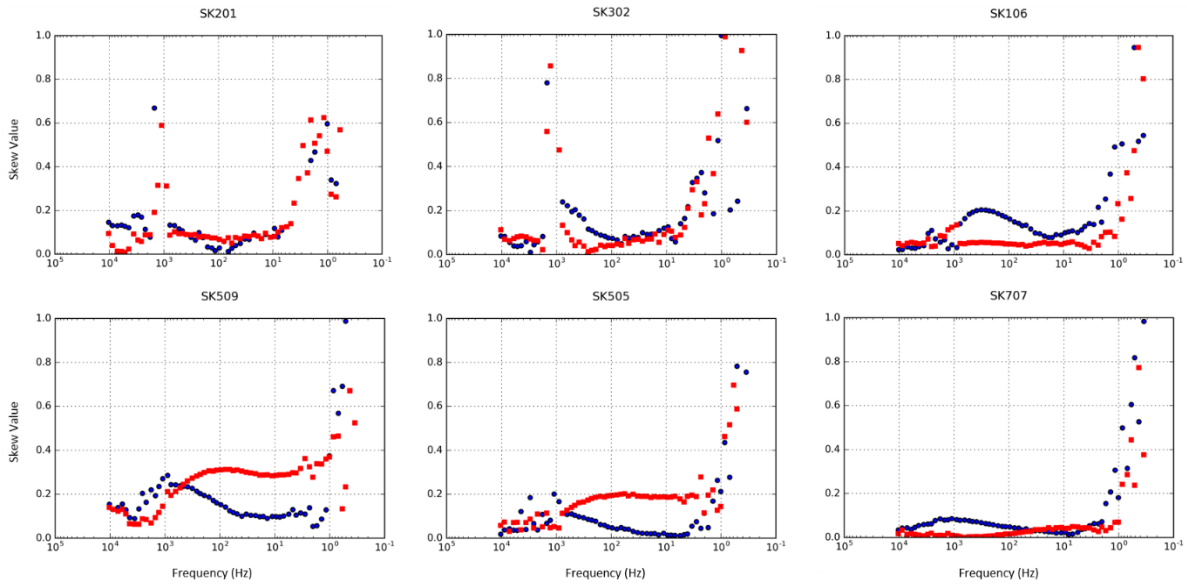

Figure 2: Swift's skew (red squared line) and ellipticity (blue circle) values for every frequency in the AMT impedance and phase tensor data. The selected stations are the one used in ANN training stage.

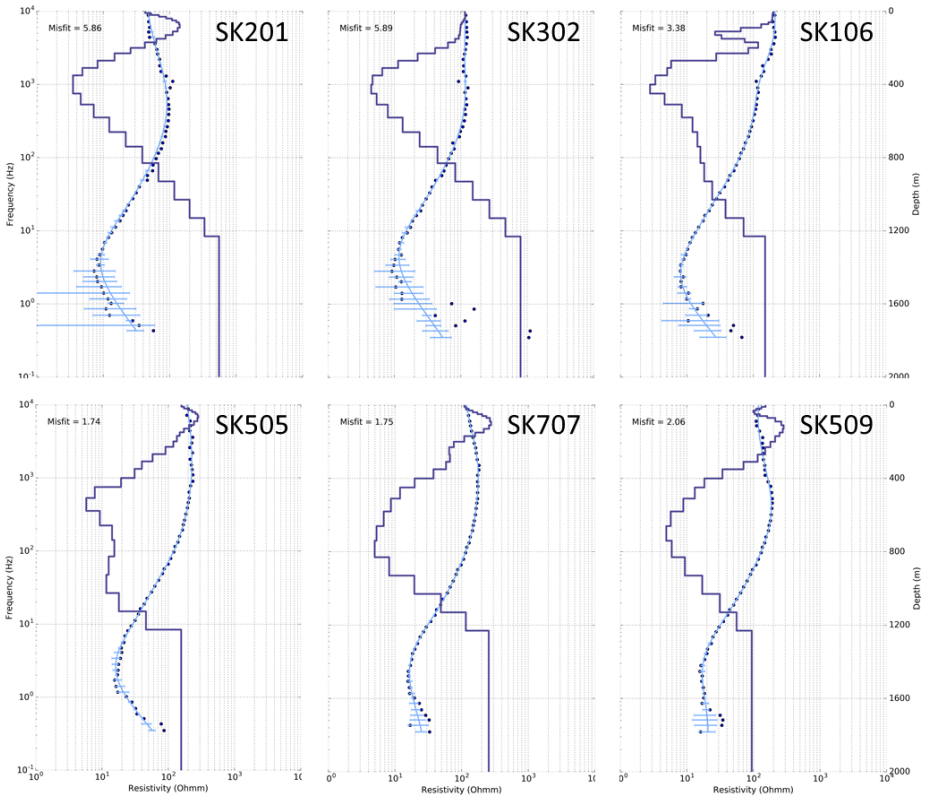

Figure 3: One-dimensional inversion results of six AMT data which were used as the learning basis (solid line is the true resistivity value, while the dotted line and thin line with error bars are the observed and the calculated apparent resistivity, respectively).

On the other hand, the thickness of this conductive layer of each station is also not similar which could be an indication of the alteration intensity occurred in the particular location as the layer is mainly formed by clay, the product of hydrothermal alteration process. The resistivity of the deeper part is much higher than the overlying clay cap which apparently suggests the zone of the porous reservoir. However, instead of merely interconnecting the 1-D resistivity structures from different AMT sites, a broader analysis should be carried out in order to conclude a comprehensive interpretation.

3. THE NEURAL NETWORK CALIBRATION

The relation between temperature of a material and its electrical characteristic have been studied extensively (see, for instance, Yokoyama et al., 1983; Llera et al., 1990; Hayashi, 2004). Most of them were agreed to the conclusion that the electrical conductivity and temperature are related exponentially. However, the empirical formula has not been revealed yet due to complex geological and hydrological behavior in the subsurface. In the electromagnetic geothermometry approach, the relationship between resistivity and temperature in every location was learned instead.

The neural network learns from the available resistivity-temperature data pairs in the training stage. To be able to predict the temperature, the ANN should modify the weight and minimize the error during the learning process, until reaching the predefined stopping criteria. To do such a task, the back-propagation algorithm was used. The input signal, containing resistivity and its coordinate, is propagating through the network to predict the temperature. Firstly, the connections inside the network were assigned with random weight values. When the estimated value is far from the expected, the signal is going back to the input layer while updating the weight based on the difference between the network output and the actual temperature value. The process iterates until the maximum iteration is reached, or stops in regards to the chosen error threshold of 10^{-5}.

It does not matter if one trains the network by using 1-D, 2-D, or 3-D resistivity model as the input information. The training result could still be used for any model, e.g., using 1-D training result to estimate the 3-D temperature distribution. It is worth mentioning that the ANN interpolation works better than ordinary methods, such as kriging interpolation (Koike et al., 2001). That finding implies that in order to make a 3-D temperature distribution model like the one attempted here, it is preferable to estimate the temperature based on the interpolated resistivity model rather than by interpolating the temperature profiles beneath each station. However, to maintain the suitability, both the training and prediction dataset need to be in the balance.

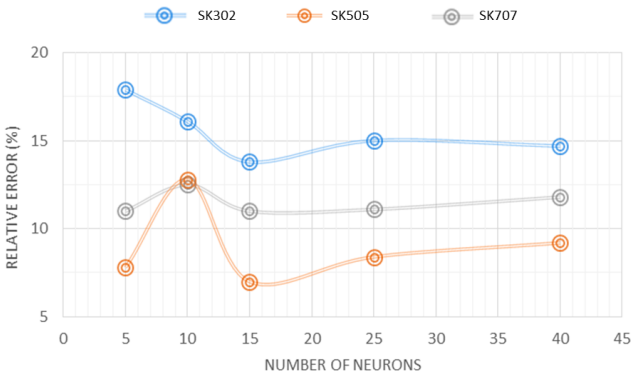

Figure 4: Relative error recorded after a prediction test as the effect of changing the number of nodes in the hidden layers.

3.1 Neuronet Training Strategy

The optimum ANN architecture was actually chosen based on trial and error. There is no exact formula to obtain the most appropriate network model because the way of learning depends highly on the problem (LeCun et al., 2012). While the number of input and output neurons was decided, the hidden neurons, as well as the employed hidden layers, were needed to be adjusted. In each trial, the network performance was evaluated from the convergence rate, time consumption, and error relative to the real value, in case the 'unseen' data is present.

For example, the effect of the number of total hidden neurons to the relative error is evaluated. After training, the calibrated network was then used to forecast the temperature in other location. The prediction outcome was compared to the actual temperature data so that the error could be calculated. The training quality was evaluated in three AMT stations as shown in Figure 4. The result is counter-intuitive as the error is not always decreasing with the number of neurons incorporated in the hidden layer. From this result, the minimum error is obtained with 15 hidden nodes, while the larger number than this leads to the slightly higher error. In this work, the ANN topology consists of 4 input nodes (i.e., resistivity, depth, latitude, and longitude), 15 hidden nodes in two hidden layers, and a single neuron containing temperature information in the output layer. Sigmoid activation function was used in each neuron.

The trained network needs to be tested to assess the quality by comparing the prediction result to the actual value of temperature in a particular location or depth. Therefore, it is necessary to have other data outside the ones used in training or keep some part of the available data unseen by the network. When the prediction accuracy is acceptable, the ANN can be used to estimate the temperature in other location. Otherwise, some re-adjustment is necessary regarding the network model or the training strategy.

3.2 Vertical and Lateral Temperature Prediction Test

Borehole thermal logging usually cannot cover a preferable depth, and performing thermal logging in a large number is costly and time-consuming. Taking advantage of sufficient penetration of electromagnetic signal in AMT survey and a large number of AMT measurement sites, the electromagnetic geothermometer was tested to extrapolate the temperature profile below the borehole up to the desired depth as well as forecasting the temperature in the inter-well spacing.

For vertical temperature extrapolation, the neural network was trained based only on depth, resistivity, and temperature value for each depth. The horizontal coordinates were not used as there was no horizontal variation. The depth and resistivity from the same AMT station were treated as nodes in the input layer, while the temperature is employed as the only output node in the output layer of the neural network training model. The shallower resistivity data was used for teaching the network. In order to evaluate the prediction accuracy, some portions of the observed temperature profile, those in the deeper part, were not used. For this purpose, only the data up to 700-800 m depth (from the total depth of 1,000-1,800 m) was exploited for training as well as validating the training result, while the rest was used to evaluate the performance of the network in extrapolating the temperature profile beneath the borehole by the percentage of the relative error (*Er*) between the estimated and measured values as follows,

$$E_r = \sqrt{\frac{\sum_{i=1}^{N}(T_{m,i} - T_{p,i})^2}{\sum_{i=1}^{N} {T_{m,i}}^2}} \times 100\%, \quad (3)$$

where $T_{m,i}$ and $T_{p,i}$ are the measured and predicted values of the i-th parameter, respectively, and N represents the number of observed temperatures.

For the vertical temperature prediction test, three resistivity-temperature data pairs were used for training and for the test as well. They are SK201-BT1, SK707-BT5, and SK509-BT6. The resistivity data used for training the network was only a part of the whole the dataset, whereas all the data, including the one previously used in training, was used as a proxy for estimating the temperature. The purpose is to get an entire idea about how the neural network performance differs from the seen and the unseen case. The result is shown in Figure 5.

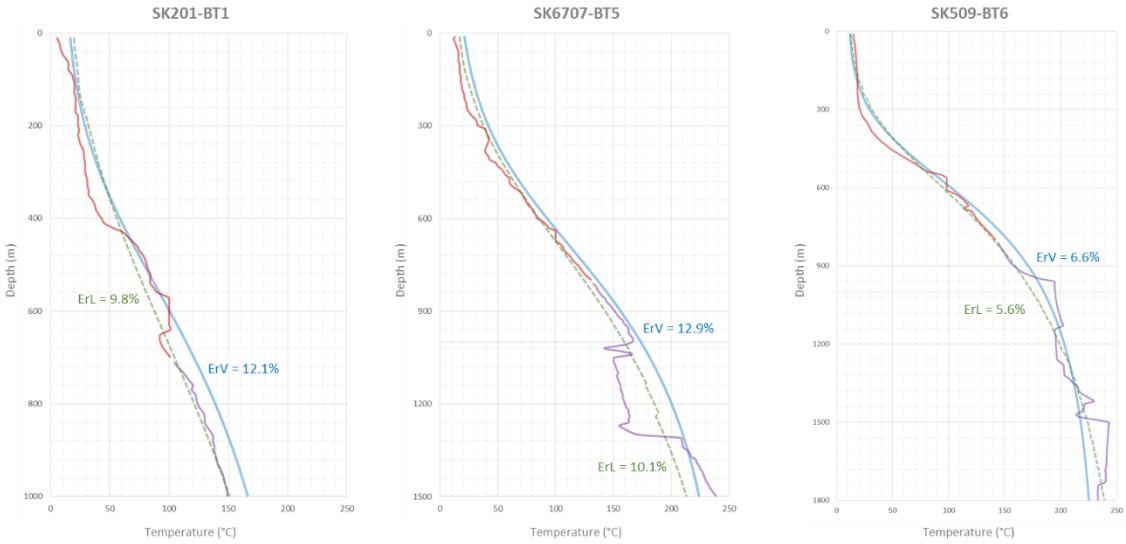

Figure 5: ANN vertical and lateral temperature prediction test result (respectively represented by a solid blue line and dotted green line), and its comparison with well-log data (solid line; red for the training data, purple for the unseen data). ErV denotes the relative error for vertical extrapolation case, while ErL indicates the error of the lateral prediction result.

The predicted portion is different for each dataset. In the first case (SK201-BT1), the data employed in training was up to 700 m, while the ANN was used to predict the temperature as deep as 1 km which is about a half of the training data length. The result was acceptable as the fit of the observed and estimated curves is good and the error is considered fine. For the second data pair, the portion of training and prediction dataset was almost 1:1. From the comparison, there is no clear difference with the previous one. However, in this particular graph, it is apparent that the network was unable to follow the actual temperature profile when there is an occurrence of sudden temperature change, e.g., at the depth range between 1,000 m and 1,300 m depth. The ANN performance in extrapolating the temperature profile was again tested using a larger amount of prediction dataset incorporated in the third data pair. With the relative error of 6.6%, the result was utterly satisfying. A small difference in the number of training data does not really affect the prediction quality, the complexity of the subsurface temperature structure does.

The trained network quality for the deeper temperature extrapolation was proven. Following this result,another test to evaluate the ability of the ANN to forecast the temperature in other location was also carried out. For this case, the network had learned the resistivity and temperature relation based on the available datasets other than the ones used for testing. The result of this test was also shown in Figure 5, denoted by the dotted green line. Note that in this case, the training data volume was significantly increased. The relative error is lower than the previous test, yet the partial temperature fluctuation remains unpredictable. This limitation may be overcome by enriching the training data variation or adding some supporting information for the network training, such as porosity, hydrothermal alteration, etc. Following all results, the ability of the trained ANN for forecasting the deeper temperature values was satisfying both qualitatively and quantitatively. Thus, the ANN was ready to estimate the temperature distribution on a larger scale.

4. RESULT AND DISCUSSION

Following a satisfying performance in the prediction test stage, the ability of the neural network to reconstruct the subsurface temperature distribution becomes promising. In order to estimate the temperature distribution for the geothermal area, a 3-D inversion of AMT data should be done in the first place.

4.1 Three-Dimensional Resistivity Model

This process was carried out through the use of ModEM 3-D MT Inversion (Kelbert et al., 2014). Input files for the code were prepared using MTpy, an open source Python toolbox for pre-processing of MT data (Krieger and Peacock, 2014). Since the diagonal impedance values of the data are not negligible, the inversion was based on full impedance data. All the 60 frequencies were included in the inversion process.

The minimum lateral cell size in the model block is 75 m × 75 m while it becomes two times longer at each padding side. Lateral interpolation grid was minimized, considering the small inter-stations distance. Surface model thickness is 10 m and elongated with depth until reaching the maximum model depth of 2 km. The vertical block was made as same as the one modeled in the previous 1-D inversion so that the depth model for both training and prediction are proportional. The inversion process stopped after 60 iterations with overall RMS error of 8.8%. Figure 6 shows the comparison between observed data and model response for four selected AMT sites. From the comparison, it is apparent that the calculated data are fit with the measured one except in the lowest frequency range, of the K02 station in particular. Small error and the curve fitness indicates that the 3-D inversion was performed successfully.

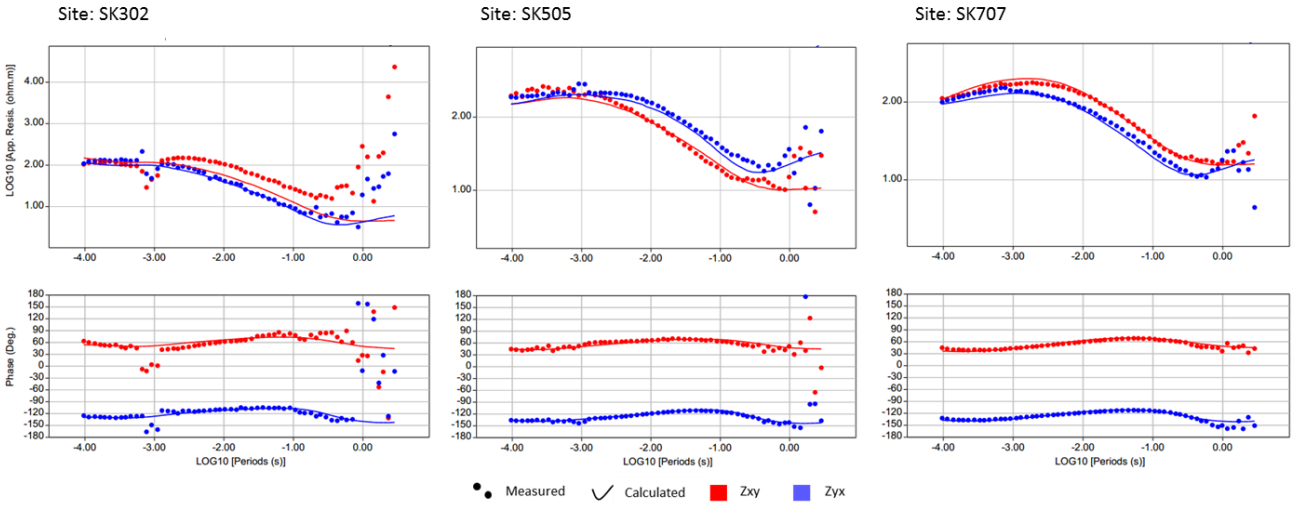

Figure 6: Comparison between the observed data (dotted line) and the 3-D model responses (solid line) for site SK302, SK505, and SK707. Red color indicates XY direction, while blue color represents YX direction.

The inversion result was sliced following one profile line at the center as shown in Figure 7. At the shallow depth, irregular shape of high resistivity anomaly is encountered. This is most probably indicating the volcanic body that covers the surface. The altered layer is detected from 500 m up to 1,500 m depth, and getting thinner in the center and towards the south. At this depth range, the occurrence of fault could be identified. The geothermal reservoir zone could be recognized from the medium resistivity anomaly which spreads evenly in the deeper part.

To evaluate the lateral extension of the resistivity anomaly, horizontal depth slices are also presented in the same figure. An interesting finding from this figure is that the conductive layer dominantly appears around the area at 500 m depth. In this part, the discontinuity of this anomaly can also be clearly seen at the center which could be detected due to the occurrence of a massive fracture system. In the subsequent layer, the conductive layer still appears in the northwestern part. This anomaly indicates a more intensive alteration occurred in this location. There is no trace of the impermeable conductive layer at the model padding sides. However, because there is no AMT data covering this area, the result recorded on the sides is less trustworthy. In the 1,500 m depth slice, the resistivity contrast is minimum which could be an indication of the appearance of a regional structure which takes a role as the reservoir body.

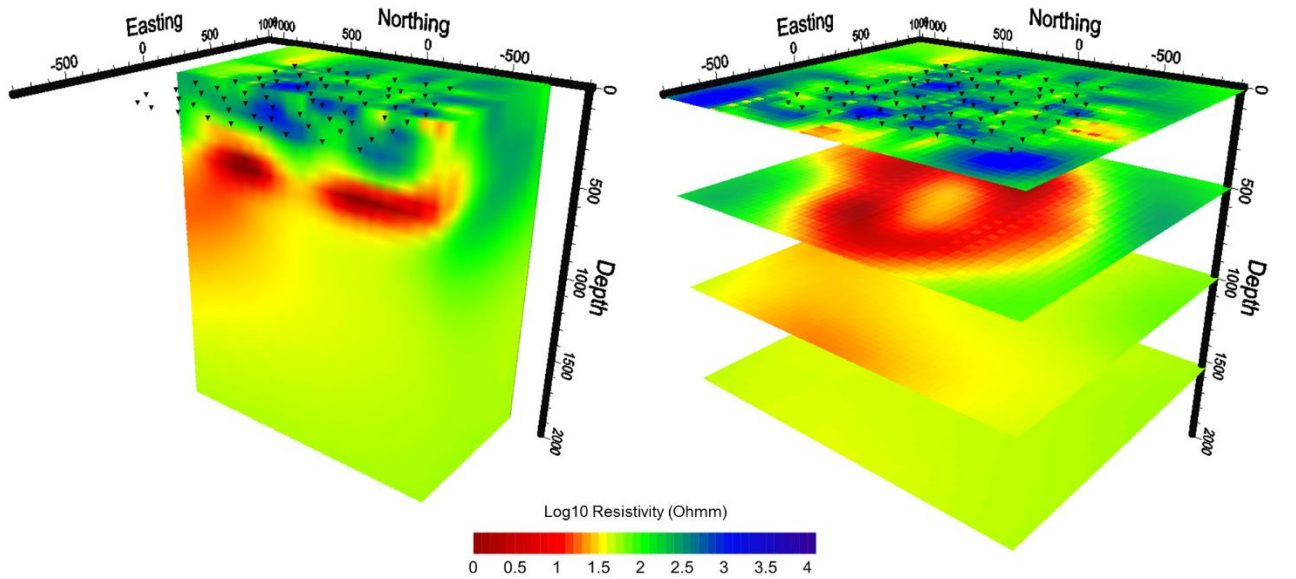

Figure 7: Resistivity block model sliced along the central profile line from north to south (left-hand side) and depth slices (at 0 m, 500 m, 1000 m, and 1500 m) of the three-dimensional AMT inversion result.

4.2 Subsurface Temperature Estimation

The subsurface heat distribution beneath the whole geothermal area was determined. By using the resistivity value resulted from ModEM 3-D inversion process, the trained ANN predicted the temperature in the same dimensionality. One of the advantages of using the back-propagation algorithm in ANN is that the time needed for prediction is short. By using the trained network and based on the result of the 3-D inversion previously, deep temperature distribution was estimated. The final estimated three-dimensional temperature map is shown in Figure 8. The coordinate system used in this figure is the local one, as used in the 3-D inversion. To ease the interpretation, scatter plots of station locations are placed on the top.

Apparent from the figure that the highest geothermal gradient detected in this area is located in the south-western part and the north-western part of the field, which could indicate the occurrence of an active heating zone. From the thermal pattern, it could be assumed that the temperature increases towards the east where the volcanic mountains stand. The gradient is lower in the middle part, and this temperature depletion continues along the east-northeast to west-southwest direction, the same orientation with the dominant fracture system explained from the geologic investigation. This could be an indication that the highly permeable fractures behave as a passageway for the cold meteoric water.

4.3 Joint Interpretation

Delineating a complete description of heat distribution within the earth's interior below the field initially is the main purpose of this work. Comprehensive information about temperature anomaly can ease the study about the existing geothermal activity, especially in terms of heat propagation analysis. Together with three-dimensional resistivity model, this temperature distribution could promote the detailed and integrated interpretation in order to obtain a proper idea about the geothermal system within the area. This joint analysis was implemented, as an additional discussion, in order to investigate the correlation between the predicted temperature distribution and the other available data, as well as to enhance the reliability of this method.

To ease the interpretation, the combined model (Figure 9) shows the vertical slice which intersects with some of the wells (BT1, BT4, and BT6) so that the information from these boreholes can also be used to enrich the analysis. One interesting finding in the figure is that the sudden depletion of temperature occurs in the same place where the fracture is detected below BT4. A thermo-remnant analysis of sample cores indicated that the well encounter a sub-fault oriented in northwest-southeast direction with a dip angle of 70° facing the south. This could be an indication that the fault acts as a feeding zone that transports cold water to the reservoir. Note that the width of the fracture described in Figure 9 is not to scale.

The high geothermal gradient encountered in the northwestern part is most probably evidence of an extensive discharge of the geothermal fluid. The same reason causes an enormous conductive zone below BT1 which could be inferred as an intensively altered zone. This assumption was also supported by the presence of small fumarole manifestations at nearly 1 km to the west from the borehole. A roughly similar situation occurred in the southeastern part of the area as recorded in BT6. The alteration seems less intense in this area since the closest manifestation is located around 3 km to the southwest, and there is no sign of fault encountered by the wellhead.

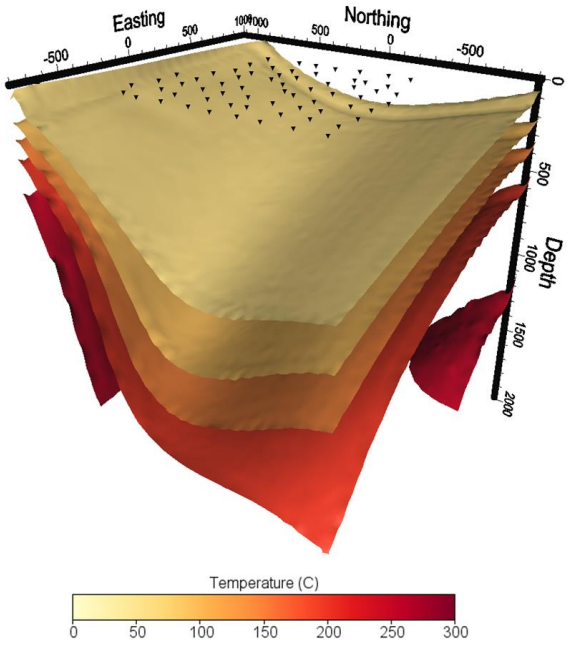

Figure 8: The predicted 3-D temperature distribution below the geothermal field presented as isotherm layers of 50, 100, 150, 200, and 250 °C.

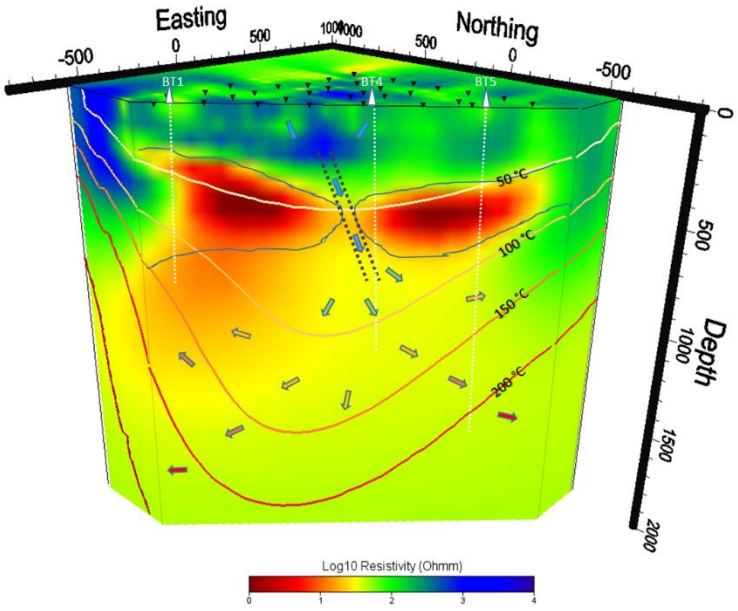

Figure 9: Conceptual model of the subsurface structure below the geothermal area constructed from 3-D resistivity and temperature distribution. Length and width of the deduced fault structure are not to scale. The arrows indicate the geothermal fluid movement while the colors represent their temperature (blue for the pre-heated fluid, red for the hot fluid).

Taking into account all the findings, it could be assumed that the reservoir body gets the cold water from the large-scale fractures in the central part which lower the temperature surrounding the sub-faults. The water is heated by the heat source through a convection mechanism occurred extensively below the area which also alters the overlying structure. The hot fluid then moves to the surface as a manifestation through the major fault system situated around the geothermal field.

5. CONCLUSIONS

The trained ANN had proven its capability to estimate the temperature at great depths up to 2 km. The result of temperature extrapolation in depth is satisfying with the average error less than 15%. Following this result, the ANN was also tested to forecast the subsurface temperature below other AMT stations. The outcome was as good as the previous test with the average error no larger than 10%. However, the ANN could only predict the main trend of the temperature profile. The present ANN strategy was unable to detect the presence of sudden temperature fluctuations. The output of the ANN prediction was also profoundly influenced by the variation of training data so that any particular unseen case would be difficult to be predicted.

The ANN test was considered successful and had shown an evident performance when applied in a more extensive temperature prediction. It is worth to mention that the dimensionality of the training data does not need to be similar to the temperature that is being predicted. In this work, the training data was only supplied by the result of 1-D resistivity data inversion and the available borehole thermogram data which is also one-dimensional. The ANN prediction performed well for each predicted model as the pattern of the estimated subsurface temperature was reasonable. Both resistivity and temperature data showed some agreement with the surface geological investigation as well as the well logging documentation. Considering all results, it is reasonable to conclude that the temperature estimation by using the trained artificial neural network is giving an acceptable result. The predicted temperature distribution can provide a lot of information about the geothermal system and significantly enhance the data interpretation. Together with some other geological, geochemical and geophysical data, this electromagnetic geothermometry can provide essential information to delineate a proper subsurface temperature model.

ACKNOWLEDGEMENTS

We acknowledge the Indonesian Endowment Fund for Education (LPDP) for the monetary support of the study presented in this conference. Our sincere thanks go to the members of Exploration Geophysics Laboratory, Kyushu University for their constructive suggestions and criticisms during discussions.

REFERENCES

Akpan, A.E., Narayanan, M., Harinarayana, T.: Estimation of Subsurface Temperatures in the Tattapani Geothermal Field, Central India, from Limited Volume of Magnetotelluric Data and Borehole Thermograms using a Constructive Back-propagation Neural Network, *Earth Interact.*, **18**, (2014), 1–26. doi:10.1175/2013EI000539.1

Bibby, H.M., Caldwell, T.G., Brown, C.: Determinable and non-determinable parameters of galvanic distortion in magnetotellurics. *Geophys. J. Int.*, **163**, (2005), 915–930. doi:10.1111/j.1365-246X.2005.02779.x

Caldwell, T.G., Bibby, H.M., Brown, C.: The magnetotelluric phase tensor. *Geophys. J. Int.*, **158**, (2004), 457–469. doi:10.1111/j.1365-246X.2004.02281.x

Constable, S.C.: Occam's Inversion: A Practical Algorithm for Generating Smooth Models from Electromagnetic Sounding Data. *Geophysics*, **52**, (1987), 289. doi:10.1190/1.1442303

Hayashi, M.: Temperature-Electrical Conductivity Relation of Water for Environmental Monitoring and Geophysical Data Inversion. *Environ. Monit. Assess.*, **96**, (2004), 119–128. doi:10.1023/B:EMAS.0000031719.83065.68

Kelbert, A., Meqbel, N., Egbert, G.D., Tandon, K.: ModEM: A Modular System for Inversion of Electromagnetic Geophysical Data. *Computer and Geoscience.*, **66**, (2014), 40–53. doi:10.1016/j.cageo.2014.01.010

Key, K.: 1D Inversion of Multicomponent, Multifrequency Marine CSEM Data: Methodology and Synthetic Studies for Resolving Thin Resistive Layers. *Geophysics*, **74**, (2009), F9–F20. doi:10.1190/1.3058434

Koike, K., Matsuda, S., Gu, B.: Evaluation of Interpolation Accuracy of Neural Kriging with Application to Temperature-Distribution Analysis. *Math. Geol.* **33**, (2001), 421–448. doi:10.1023/A:1011084812324

Krieger, L., Peacock, J.R.:. MTpy: A Python Toolbox for Magnetotellurics. *Computer and Geoscience*, **72**, (2014), 167–175. doi:10.1016/j.cageo.2014.07.013

LeCun, Y.A., Bottou, L., Orr, G.B., Muller, K.R.: Efficient Backprop. *Lect. Notes Comput. Sci*, (2012), 9–48. doi:10.1007/978-3-642-35289-8-3

Llera, F.J., Sate, M., Nakatsuka, K., Yokoyama, H.: Temperature Dependence of the Electrical Resistivity of Water-Saturated Rocks. *Geophysics*, **55**, (1990), 576-585.

Maryadi, M., Mizunaga, H.: Analysis of Audio-frequency Magnetotelluric Data for Three-Dimensional Deep Temperature Reconstruction, *Proceedings*, International Symposium on Earth Science and Technology, Fukuoka, Japan, (2017), 68–71.

Spichak, V. V.: Estimating Temperature Distributions in Geothermal Areas Using a Neuronet Approach. *Geothermics*, **35**, (2006), 181–197. doi:10.1016/j.geothermics.2006.01.002

Spichak, V. V., Zakharova, O.K.: The Application of an Indirect Electromagnetic Geothermometer to Temperature Extrapolation in Depth. *Geophysical Prospecting*, (2009). 653–664. doi:10.1111/j.1365-2478.2008.00778.x

Spichak, V. V., Zakharova, O.K.: Electromagnetic Geothermometry. *Springer*, (2015). doi:10.1016/C2014-0-01908-9

Spichak, V. V., Zakharova, O.K., Rybin, A.K.: Methodology of the Indirect Temperature Estimation Basing on Magnetotelluric Data: Northern Tien Shan Case Study. *J. Appl. Geophys*, **73**, (2011), 164–173. doi:10.1016/j.jappgeo.2010.12.007

Swift, C.M.: A Magnetotelluric Investigation of an Electrical Conductivity Anomaly in the Southwestern United States. *Ph.D. Dissertation*, (1967), 211.

Yokoyama, H., Nakatsuka, K., Abe, M., Watanabe, K.: Temperature Dependency of Electrical Resistivity of Water Saturated Rocks and the Possibility of Underground Temperature Estimation. *J. Geotherm. Res. Soc. Japan*, **5**, (1983), 100–120.